Modeling the Interaction of Laser-Produced Proton Beams with Matter

Jack McKee
Mathematics
University of Hawai'i at Mānoa
Honolulu, HI, USA
email: jmckee@math.hawaii.edu

David Eder
Physics and Astronomy
University of Hawai'i at Mānoa
Honolulu, HI, USA
email: dceder@hawaii.edu

Aaron Fisher
Information Technology Services
University of Hawai'i at Mānoa
Honolulu, HI, USA
email: fallen@andcheese.org

Alice Koniges
Information and Computer Sciences
University of Hawai'i at Mānoa
Honolulu, HI, USA
email: koniges@hawaii.edu

Claudia Parisuaña
Department of Mechanical Engineering
Stanford University
Stanford, CA USA
email: cparisua@stanford.edu

Maxence Gauthier
SLAC National Accelerator Laboratory
Stanford University
Menlo Park, CA USA
email: gauthier@slac.stanford.edu

Emma Elizabeth McBride
SLAC and School of Math & Physics
Queen's University Belfast
Belfast BT7 1NN, UK
email: e.mcbride@qub.ac.uk

Frank Seiboth
Deutsches Elektronen-Synchrotron DESY
Research Centre of the Helmholtz Association
22607 Hamburg, Germany
email: frank.seiboth@desy.de

Chandra Breanne Curry
SLAC National Accelerator Laboratory
Stanford University
Menlo Park, CA USA
email: ccurry@slac.stanford.edu

Mungo Frost
SLAC National Accelerator Laboratory
Stanford University
Menlo Park, CA USA
email: mdfrost@slac.stanford.edu

Eric Galtier
SLAC National Accelerator Laboratory
Stanford University
Menlo Park, CA USA
email: egaltier@slac.stanford.edu

Siegfried Glenzer
SLAC National Accelerator Laboratory
Stanford University
Menlo Park, CA USA
email: glenzer@slac.stanford.edu

***Abstract*—The paper reports on efforts to significantly increase our understanding of isochoric heating of matter using laser-produced proton beams, and the associated High Energy Density (HED) and Warm Dense Matter (WDM) regimes generated. This will benefit research fields such as planetary science, fusion energy, plasma physics, long-term battery storage, qubit synthesis, and material science. We discuss our experiments that irradiated Si targets with proton beams generated by the 20 TW-laser at the SLAC MEC end-station, Linac Coherent Light Source (LCLS), SLAC National Accelerator Laboratory. The HED/WDM states are probed using the 50 fs hard X-rays using the fundamental undulator harmonic of LCLS. We compare our results from the phase contrast X-ray imaging, which shows the generation of compression waves that produces rear surface spallation, to modeling results from the 3D multi-physics multi-material code, PISALE, that combines Arbitrary Lagrangian-Eulerian (ALE) hydrodynamics with Adaptive Mesh Refinement (AMR). This comparison required modifications to several physics models in the PISALE (Pacific Island Structured-AMR with ALE) code.**

Keywords-Adaptive Mesh Refinement; Computational Fluid Dynamics; Arbitrary Lagrangian Eulerian Methods; High Performance Computing; isochoric heating; Phase Contrast Microscopy; X-ray Diffraction; X-ray Free Electron Lasers.

I. INTRODUCTION

Increasing our understanding of isochoric (constant volume) heating of matter and the associated High Energy Density (HED) and Warm Dense Matter (WDM) [1][2][3] generated regimes using laser-produced proton beams [4][5][6] will benefit research in many fields, such as planetary science [7], fusion energy [8][9][10][11][12][13][14], plasma physics [15][16][17][18], long-term battery storage, qubit synthesis [19], and material science [20]. For example, it will enhance our understanding of WDM properties of iron and silica under conditions encountered in planetary interiors and diagnostic components in fusion devices exposed to high fluxes of energetic plasma ions. The work is also relevant to long-term battery storage using Si. Short-pulse laser-produced ion beams can create chains of closely coupled qubits based on "color centers" in diamond and other material [19].

We present results of experiments that irradiated Si targets, at near constant density to eV temperatures, with proton beams generated by the 20 TW-laser at the Matter in Extreme Conditions (MEC) end-station at the Linac Coherent Light Source (LCLS) located at the SLAC National Accelerator Laboratory. This short-lived high-temperature, high-density state is probed using the 50 fs hard X-rays using the fundamental undulator harmonic of LCLS. The results of the phase-contrast X-ray imaging indicate ion energy deposition inside the 20 μm thick Si target, and the subsequent evolution reveals the generation of compression waves that reflect off the rear surface resulting in intense tensile stress and spallation.

In this paper, we also discuss the development and use of the PISALE code to model our experiments. The 3D multi-physics multi-material code, PISALE, combines Arbitrary Lagrangian-Eulerian (ALE) hydrodynamics with Adap-

tive Mesh Refinement (AMR). The PISALE (Pacific Island Structured-AMR with ALE) code has physics models that include laser/ion deposition, radiation hydrodynamics, thermal diffusion, anisotropic material strength with material time history, advanced models for fragmentation, and surface tension models. The PISALE code has an ion beam deposition package that has been used to model Li ions. In some earlier papers (e.g., [21]), the PISALE code is called ALE-AMR as it was one of the first codes to combine those two methods.

Modeling new experimental configurations generally requires modifications to the code in addition to determining new parameters for the various models that are used in the simulations. One advantage of PISALE over some codes used to model US Depsrtment of Energy (DOE) funded experiments, is that graduate students and postdocs can modify the source for a particular experiment [22].

In section II, we provide a brief background of the PISALE code and the equations that are solved. In section III, we discuss improvements to the code that are need to model ion beam experiments with a range of ion energies. In section IV, we provide details of our experiment using laser-produced protons to heat a Si target. In section V, we discuss PISALE simulations of our experiment. In section VI, we provide conclusions and discuss future work.

II. PISALE Code Background

PISALE operates on top of the scalable Structured-AMR Application Infrastructure (SAMRAI) library [23]. The PISALE code contains a general purpose PDE solver that uses a staggered-grid, Lagrangian formulation, written for coupled plasma/fluids with position and velocity being nodal variables and density, internal energy, temperature, pressure, strain, and stress being zonal (cell centered) variables. These plasma/fluid equations in a Lagrangian formulation (in vector and indicial notation $i, j, k = 1, 2, 3$) are:

$$\frac{\mathrm{D}\rho}{\mathrm{D}t} = -\rho\nabla\cdot\vec{U} = \rho U_{i,i} \quad (1)$$

$$\frac{\mathrm{D}\vec{U}}{\mathrm{D}t} = \frac{1}{\rho}\nabla\cdot\boldsymbol{\sigma} = \frac{1}{\rho}\sigma_{ij,j} \quad (2)$$

$$\frac{\mathrm{D}e}{\mathrm{D}t} = \frac{1}{\rho}V\boldsymbol{s}:\dot{\boldsymbol{\varepsilon}} - P\dot{V} = \frac{1}{\rho}V\left(s_{ij}\dot{\varepsilon}_{ij}\right) - P\dot{V} \quad (3)$$

where $\frac{\mathrm{D}}{\mathrm{D}t} = \frac{\partial}{\partial t} + \vec{U}\cdot\nabla$ is the substantial derivative, ρ is the density, $\vec{U} = (u, v, w)$ is the material velocity, t is time, $\boldsymbol{\sigma}$ is the total stress tensor, P is the pressure, e is the internal energy, V is the relative volume ($\rho V = \rho_0$ where ρ_0 is the reference density), $\boldsymbol{s}$ is the deviatoric stress defined as $s_{ij} = \sigma_{ij} + P\delta_{ij}$ where δ is the Kronecker delta and $\dot{\boldsymbol{\varepsilon}}$ is the strain rate tensor. PISALE has a range of different strength and failure models.

Thermal conduction and radiation transport coupled to the basic conservation law equations are solved by implementing the diffusion approximation, which uses a nodal radiation energy and a zone-averaged nodal temperature [24]. The original PISALE Finete Element Method (FEM) package includes only first order H^1 quadrilateral and hexahedron elements in 2D and 3D. This works well for the diffusion equation solvers utilized in the heat conduction and radiation diffusion modules. The original FEM package in PISALE only supports AMR in 2D. We are currently coupling PISALE to the Modular Finite Element Methods (MFEM) library [25]. This will provide a wide variety of powerful FEM-based PDE solvers, with the added benefit of support for GPU acceleration, automatic differentiation, high-order methods and more including the support of AMR in 3D simulations.

III. Recent Improvements to PISALE to Model Ion-Beam Experiments

In order to model our experiments using laser-produced ion beams, we evaluated and extended the ion-beam package in PISALE. Previous work using the package was restricted to a monoenergetic beam of Li ions. We have modified the ion-beam package in PISALE to have multiple ion beams with different ion properties, including ion energy, spot size, and fluences as a function of time. The PISALE code exploits complex numerical techniques for fully anisotropic stress tensors, interface reconstruction for multiple materials, and a flexible strength/failure infrastructure for analytic or tabulated material models and equations of state. We have determined the appropriate equation of state and material strength/failure model for the Si material used in our experiments. In the PISALE code, a void material with an associated volume fraction is introduced when a material failure occurs. This can result in spall planes that will be compared to measured spall generation.

IV. Experiments Details using Laser-Produced Proton Beams

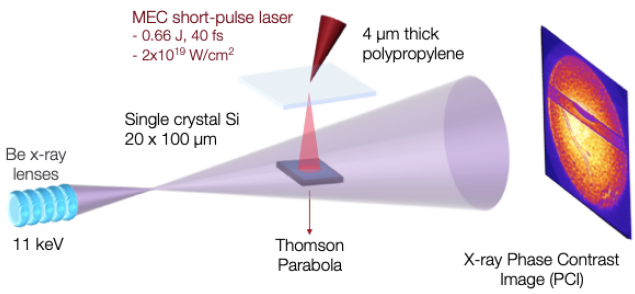

Figure 1. Experimental configuration using proton beams generated by the 20 TW-laser at the SLAC MEC end-station to heat a Si target.

Laser-produced high-energy (MeV) proton beams can be used for isochoric heating of solid targets [26][27][28]. In our experiment, the 0.66 J, ~50 fs, 800 nm Ti:Sapphire MEC pump laser (P-polarized) was focused onto a 4 μm-thick propylene foil using an f/6 off-axis parabola, reaching peak intensities of ~2×10^{19} W/cm^2. Interaction with the solid-density target generated a population of hot electrons, a fraction of which escaped from the rear surface, forming a strong electrostatic sheath field. This field accelerates surface ions via the Target Normal Sheath Acceleration (TNSA) mechanism [29], producing a well-collimated proton beam normal to

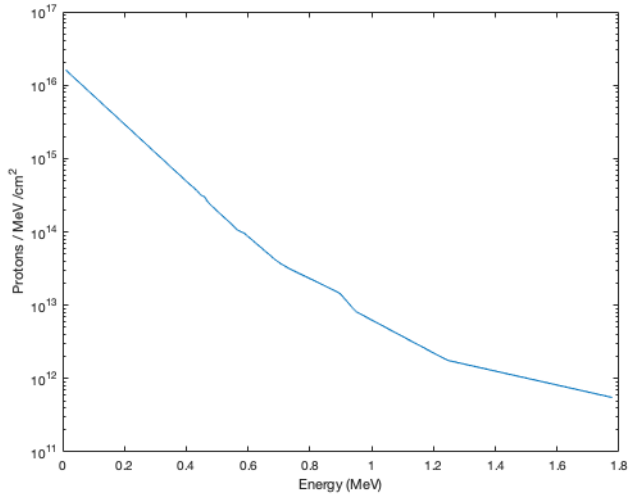

Figure 2. Measured proton spectrum generated by the 20 TW-laser striking polypropylene target.

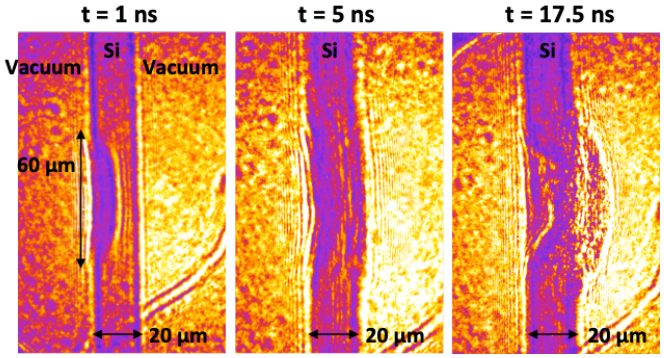

Figure 3. Measured response in Si target from proton beam arriving from the left.

the target. A secondary sample—20 μm-thick single-crystal silicon—was placed 300–500 μm from the proton source, where the ions deposited most of their energy at the end of their range, resulting in isochoric heating. The experimental set-up is shown in Figure 1. This short-lived warm dense matter state sample is imaged using the 50 fs, 11 keV X-ray LCLS beam. The proton spectrum and angular distribution produced during the interaction were measured using an absolutely calibrated Thomson parabola spectrometer and a stack of RadioChromic Films (RCFs). The measured proton spectrum is shown in Figure 2. The combination of the high intensity short pulse laser system at MEC, able to create MeV proton beams to isochorically heat matter, with the LCLS, allows unprecedented access to the creation and interrogation of this exotic state of matter.

The heated target was spatially and temporally diagnosed using the MEC X-ray Imager (MXI), operated in a Phase-Contrast Imaging (PCI) configuration [30]. The collimated 11 keV LCLS beam was prefocused upstream of the sample using a stack of 40 beryllium Compound Refractive Lenses (CRLs), generating a secondary x-ray source located 214 mm before the sample. The transmitted x-rays were recorded on a YAG phosphor screen positioned 4901 mm downstream. This screen was re-imaged by a high-resolution optical system coupled to an sCMOS camera using a 1.8 x magnification objective, yielding a total geometric magnification of 42 and an effective pixel size of approximately 150 nm.

Typical experimental results are shown in Figure 3. The MeV proton beam arrives at the target from the left. These measurements visualize the density evolution as a function of time starting with the firing of the short-pulse laser. The generated protons travel to the Si target with the highest energy ones arriving first. One nanosecond after the pump laser irradiates the polypropylene target and starts producing the proton beam, we observe the effects of proton-induced energy deposition (left image). At 5 ns (center image) we see the generation of a compression wave. At 17.5 ns (right image), we see material failure and spallation. In another experiment, we observed similar spallation in Ge foils using a 20 ns laser pulse to generate the shock [30].

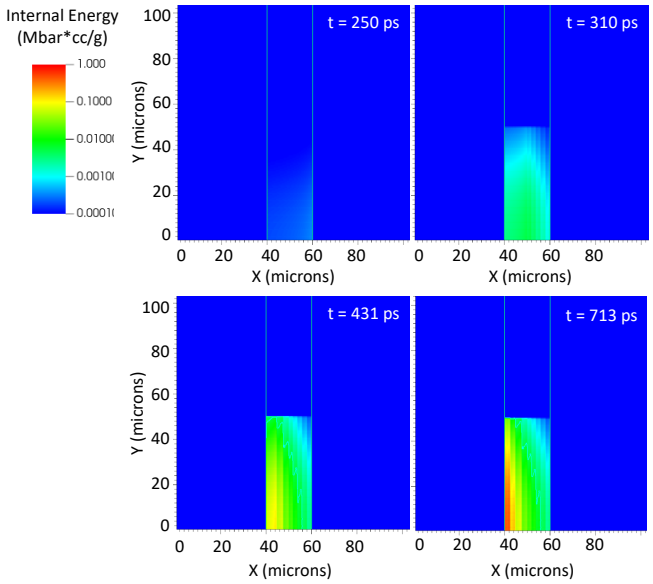

Figure 4. Calculated internal energy per unit mass of 20 μm thick Si target heated by proton beam arriving from the left at four times.

V. PISALE Simulation Results

Simulations of our experiments can provide insight into the properties of the Si target and the cause of the observed spallation. We use the measurements of the proton spectrum, shown in Figure 2, as input for our PISALE simulations. We split energies into fixed-width ranges based on the individual proton energies, and for each bin we calculated a beam intensity that matchs the total deposited energy of that bin determined by integrating an exponential fit of the curve in Figure 2. The arrival time at the Si sample is a function of their energy, with the highest energy ones arriving first. Given

the relatively small distance between the foil where the protons are produced and the Si targets, all the protons arrive before any significant hydrodynamics motion occurs. This results in isochoric heating by the protons. We divide the protons into different energy groups with corresponding different arrival times. In addition to arriving at different times, the ions with different energies deposit their energy at different locations in the Si sample. We explored using different numbers of energy groups, and the results shown in this report are for 17 energy groups going from 0.05 to 1.8 MeV with almost 60% of the energy in the proton beam being in the 0.2 to 0.6 MeV energy range. Less than 10% of the proton beam energy is below 0.2 MeV.

In general, the most important aspect of proton beams having a wide range of energies is the location of the deposited energy. In Figure 4, we show results from the PISALE simulation for the internal energy per unit mass inside the 20 μm thick Si target heated by the 50 μm radius proton beam coming from the left. The proton beam is centered on 0 in the Y axis. We model just the top half the Si target given that the target and proton beam are symmetric in Y. [These results are for a distance of 4 mm between the polypropylene foil and the Si sample, which is larger than the distance of 300 μm discussed in the previous experimental section.] The first image is at 250 ps when only protons with energy greater than 1.3 MeV have started to arrive at the target. One can see a small amount of heating in the center of the beam. Note the log scale. The next image is at 310 ps, with heating seen in the entire beam with the deposition relatively uniform through the thickness of the Si target. This is expected for these high-energy protons. At 431 ps, some of the lower-energy protons with shorter stopping distances start to arrive, and we see a higher internal energy on the front side of Si target. In the far right image, we show results at 713 ps when protons in the lowest-energy group have started to arrive, and most higher-energy protons have deposited their energy or have passed through the Si target.

The high internal energy near the front side of the target causes a shock to form and move to the right before significant hydrodynamic motion. The calculated response of the Si target to proton-beam heating is shown in Figure 5, where we show the density, with a linear scale, at four times. All the energy deposition has essentially competed by 1 ns. In the far left image at 1.4 ns, we see the shock moving to the right with a narrow density enhancement location about 3 μm into the Si target in the center of the beam path. In the next image at 2 ns, the density enhancement has broadened and is about 7 μm into the Si target. This corresponds to a velocity of 6.7 μm/ns. This is consistent with the observed velocity obtained from images at 1 and 5 ns in Figure 3. The start of rear surface motion in the simulation is seen in the 6 ns image in Figure 4. Rear-surface spall is seen in the image on the far right at 9 ns with some melting of the Si target. The rear-surface spall is calculated to start earlier than is observed. These PISALE simulations are in good agreement with the experimental data for the location of deposition and the measured shock speed. The simulation and the experiment both have rear-surface spall with the simulation having onset of spall approximately 2X sooner than the experiment.

As already stated, these simulation results are for a flight distance of 4 mm for protons, as compared to 300 μm in the experiment. For a closer distance of 300 μm, all of the proton energy will be deposited in approximately 100 ps. Given that there is little volume change in the first nanosecond, we expect the Si response, including the spall, to be similar. Another reason for expecting a similar Si response is that the location of proton deposition within the Si target is primarily a function of the proton energy, which is independent of the flight distance of the protons.

VI. Conclusions and Future Work

The project has expanded the capability of the PISALE code to model complex ion beams with varying energies, arrival times, and other beam properties. This is beneficial for ongoing modeling efforts in modeling laser-produced ion for the formation of color centers relevant to photon qubits and studying new materials for long-term battery storage. We plan to study the effect of smaller flight distance and subsequent shorter energy deposition times. We also plan to explore the effects of different equation-of-state tables/models and strength models for Si on the simulation of spallation.

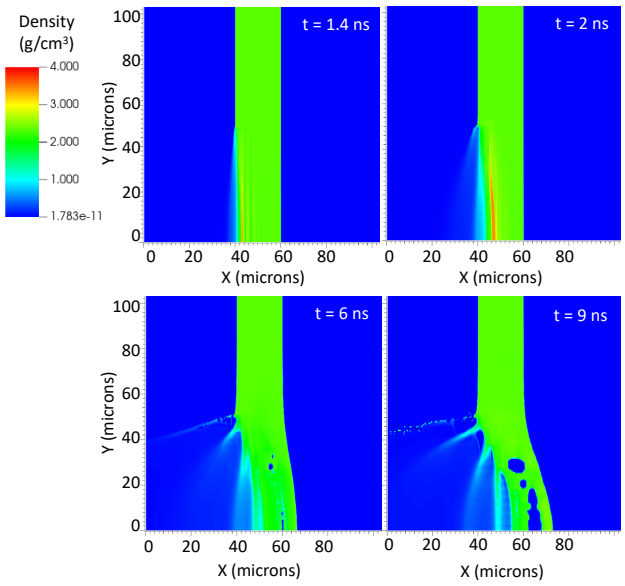

Figure 5. Calculated response of 20 μm thick Si target following heating by proton beam at four times.Measured response in Si target from MeV proton beam arriving from the left.

Acknowledgment

We would like to acknowledge the support and contributions of Z. Chen, A. Descamps, G. Dyer, L.B. Fletcher, G.D. Glenn, J. Hastings, P. Heimann, J.B. Kim, M. Mo, B. Ofori-Okai, and F. Treffert from SLAC National Accelerator Laboratory, and C. Spindloe from the Central Laser Facility, for their

involvement in the experimental campaign. This work is supported by the U.S. Department of Energy, Office of Science, under Fusion Energy Sciences Research Division Award Numbers DE-SC0023475 and DE-SC0024403, and through through FWP100182, as well as under Science Foundations for the Energy Earthshots Award Number DE-SC0024728. This research used resources of the National Energy Research Scientific Computing Center (NERSC), a U.S. Department of Energy Office of Science User Facility located at Lawrence Berkeley National Laboratory, operated under Contract No. DE-AC02-05CH11231. This work was also supported by the UK Research & Innovation Future Leaders Fellowship (MR/W008211/1).

REFERENCES

[1] P. Patel *et al.*, "Isochoric heating of solid-density matter with an ultrafast proton beam," Physical review letters, vol. 91, no. 12, p. 125 004, 2003.

[2] R. Snavely *et al.*, "Laser generated proton beam focusing and high temperature isochoric heating of solid matter," Physics of Plasmas, vol. 14, no. 9, p. 092 703, 2007.

[3] S. Malko *et al.*, "Proton stopping measurements at low velocity in warm dense carbon," Nature Communications, vol. 13, no. 1, p. 2893, 2022.

[4] S. P. Hatchett *et al.*, "Electron, photon, and ion beams from the relativistic interaction of petawatt laser pulses with solid targets," Physics of Plasmas, vol. 7, no. 5, pp. 2076–2082, 2000.

[5] E. Clark *et al.*, "Energetic heavy-ion and proton generation from ultraintense laser-plasma interactions with solids," Physical Review Letters, vol. 85, no. 8, p. 1654, 2000.

[6] S. Wilks *et al.*, "Energetic proton generation in ultra-intense laser–solid interactions," Physics of plasmas, vol. 8, no. 2, pp. 542–549, 2001.

[7] R. Smith *et al.*, "Ramp compression of diamond to five terapascals," Nature, vol. 511, no. 7509, pp. 330–333, 2014.

[8] D. A. Callahan-Miller and M. Tabak, "Progress in target physics and design for heavy ion fusion," Physics of Plasmas, vol. 7, no. 5, pp. 2083–2091, 2000.

[9] I. Hofmann, "Review of accelerator driven heavy ion nuclear fusion," Matter and Radiation at Extremes, vol. 3, no. 1, pp. 1–11, 2018.

[10] M. Roth *et al.*, "Fast ignition by intense laser-accelerated proton beams," Physical review letters, vol. 86, no. 3, p. 436, 2001.

[11] J. C. Fernandez *et al.*, "Fast ignition with laser-driven proton and ion beams," Nuclear fusion, vol. 54, no. 5, p. 054 006, 2014.

[15] M. Borghesi *et al.*, "Electric field detection in laser-plasma interaction experiments via the proton imaging technique," Physics of Plasmas, vol. 9, no. 5, pp. 2214–2220, 2002.

[16] L. Romagnani *et al.*, "Dynamics of electric fields driving the laser acceleration of multi-mev protons," Physical review letters, vol. 95, no. 19, p. 195 001, 2005.

[12] M. Key *et al.*, "Proton fast ignition," Fusion science and technology, vol. 49, no. 3, pp. 440–452, 2006.

[13] M. Roth *et al.*, "Proton acceleration experiments and warm dense matter research using high power lasers," Plasma Physics and Controlled Fusion, vol. 51, no. 12, p. 124 039, 2009.

[14] O. Hurricane *et al.*, "Approaching a burning plasma on the nif," Physics of Plasmas, vol. 26, no. 5, p. 052 704, 2019.

[17] J. Fuchs *et al.*, "Comparative spectra and efficiencies of ions laser-accelerated forward from the front and rear surfaces of thin solid foils," Physics of plasmas, vol. 14, no. 5, p. 053 105, 2007.

[18] K. Quinn *et al.*, "Laser-driven ultrafast field propagation on solid surfaces," Physical review letters, vol. 102, no. 19, p. 194 801, 2009.

[19] W. Redjem *et al.*, "Defect engineering of silicon with ion pulses from laser acceleration," Communications Materials, vol. 4, no. 1, p. 22, 2023.

[20] M. Roth *et al.*, "Energetic ions generated by laser pulses: A detailed study on target properties," Physical Review Special Topics-Accelerators and Beams, vol. 5, no. 6, p. 061 301, 2002.

[21] A. Koniges *et al.*, "Multi-material ale with amr for modeling hot plasmas and cold fragmenting materials," Plasma Sci. and Technol., vol. 17, pp. 117–128, 2015.

[22] A. Koniges *et al.*, "A survey of recent applications of the pisale code and pde framework," ADVCOMP 2023, The Seventeenth International Conference on Advanced Engineering Computing and Applications in Sciences, p. 20, 2023.

[23] B. T. N. Gunney and R. W. Anderson, "Advances in patch-based adaptive mesh refinement scalability," Journal of Parallel and Distributed Computing, vol. 89, pp. 65–84, 2016.

[24] A. C. Fisher *et al.*, "Modeling heat conduction and radiation transport with the diffusion equation in NIF ALE-AMR," Journal of Physics: Conference Series, vol. 244, p. 022 075, 2010.

[25] Mfem, https://mfem.org/, Accessed: 2025-07-11.

[26] C. McGuffey *et al.*, "Focussing protons from a kilojoule laser for intense beam heating using proximal target structures," Scientific reports, vol. 10, no. 1, p. 9415, 2020.

[27] A. Mancic *et al.*, "Isochoric heating of solids by laser-accelerated protons: Experimental characterization and self-consistent hydrodynamic modeling," High Energy Density Physics, vol. 6, no. 1, pp. 21–28, 2010.

[28] M. Carrié, P. Combis, and E. Lefebvre, "Isochoric heating with laser-accelerated proton beams," Physics of Plasmas, vol. 17, no. 12, p. 122 707, 2010.

[29] R. Snavely *et al.*, "Intense high-energy proton beams from petawatt-laser irradiation of solids," Physical review letters, vol. 85, no. 14, p. 2945, 2000.

[30] F. Seiboth *et al.*, "Simultaneous 8.2 kev phase-contrast imaging and 24.6 kev x-ray diffraction from shock-compressed matter at the lcls," Applied Physics Letters, vol. 112, no. 22, 2018.